Topics in Catalysis (2020) 63:152–165
https://doi.org/10.1007/s11244-019-01213-x

ORIGINAL PAPER

# Effect of La Addition on the Performance of Three-Way Catalysts Containing Palladium and Rhodium

**Aleksey A. Vedyagin[1] · Roman M. Kenzhin[1] · Mikhail Yu. Tashlanov[1,2] · Evgeny A. Alikin[3] · Vladimir O. Stoyanovskii[1] · Pavel E. Plyusnin[2,4] · Yury V. Shubin[2,4] · Ilya V. Mishakov[1,2] · Mikhail Yu. Smirnov[1] · Alexander V. Kalinkin[1] · Valerii I. Bukhtiyarov[1,2]**

Published online: 2 January 2020


**Abstract**
Three-way catalysts containing palladium and/or rhodium were prepared using $\gamma Al_2O_3$ doped with lanthanum oxide as a support. All the samples were obtained by an incipient wetness impregnation of the support with an aqueous solution of nitrates. In order to investigate the metal–support interaction, the support was additionally calcined at 800 °C before the impregnation procedure. Characterization of the support thermally treated within a range of 600–1000 °C by low-temperature nitrogen absorption, X-ray diffraction analysis, and electron paramagnetic resonance spectroscopy has revealed that the treatment conditions strongly affect the textural properties, the phase composition and the concentration of electron-donor sites on the surface of the support. Deposition of metals by the impregnation of initial support with a joint solution of Pd and Rh nitrates has led to formation of small Pd–Rh alloyed nanoparticles with strong metal–metal interaction, which was confirmed by a testing reaction of ethane hydrogenolysis. No alloy formation was observed in the case of mechanical mixing of the separately prepared Pd-only and Rh-only catalysts as well as in the case of preliminary calcined support impregnated with a joint solution of Pd and Rh nitrates. Bimetallic Pd–Rh catalyst of alloyed type was shown to be the most promising in terms of catalytic performance and thermal stability.

**Keywords** Three-way catalysts · Bimetallic Pd–Rh alloys · La-doped alumina support · Metal–support interaction · Thermal stability

## 1 Introduction

Since 1980s, three-way catalysts (TWC) are efficiently used as exhaust emission abatement systems to purify the gasoline engine exhaust gases providing simultaneous oxidation of CO and unburnt hydrocarbons, and reduction of nitrogen oxides [1–6]. Modern TWC are mostly represented by a complex composition of various oxide supports ($Al_2O_3$, $ZrO_2$, $La_2O_3$, $CeO_2$, etc.) with deposited precious metals (Pd, Pt, Rh) [2, 4, 6–16]. Platinum and palladium are known to exhibit superior activity in oxidation reactions [17–24], while rhodium responsibility is $NO_x$ reduction [25]. Being supported on the oxide carriers in the form of disperse nanoparticles, small clusters or even single atoms, all these metals interact with the surface of the support, and the strength of such interaction depends on the surface and bulk properties of the exact oxide [22, 26–34]. For instance, palladium deposited on pure $\gamma$-$Al_2O_3$ and $ZrO_2$ supports was reported to be stabilized on electron-donor sites on the surface in the form of small clusters, when metal loading does not exceed 0.5–0.8 wt% [35–37]. At larger Pd loadings, surface migration of palladium species occurs, thus resulting in agglomeration process and appearance of quite large Pd particles, particularly after aging at elevated temperatures. Another type of strong metal–support interaction was observed for Rh-containing catalysts. Thus, in the case of $\gamma$-$Al_2O_3$, rhodium ions $Rh^{3+}$ being formed under the reaction

✉ Aleksey A. Vedyagin
vedyagin@catalysis.ru

1 Boreskov Institute of Catalysis SB RAS, Novosibirsk, Russian Federation 630090

2 National Research Novosibirsk State University, Novosibirsk, Russian Federation 630090

3 Ecoalliance LLC, Novouralsk, Russian Federation 624131

4 Nikolaev Institute of Inorganic Chemistry SB RAS, Novosibirsk, Russian Federation 630090

conditions diffuse into the bulk of the support, where initiate local phase transformation and formation of corundum phase [38]. An encapsulation of $Rh^{3+}$ ions within this phase makes such process of deactivation irreversible. In the case of $CeO_2$-based supports, rhodium ions diffused onto the bulk, on the one hand, cause appearance of areas with increased compaction of the support, but, on the other hand, facilitate an improvement of the oxygen storage capacity [33]. Moreover, catalysts deactivated due to strong rhodium-ceria interaction can be reactivated by high-temperature oxidative treatment [39].

In order to prevent the undesirable metal–support interactions, like in the case of Rh/γ-$Al_2O_3$, and to stabilize the catalyst towards high-temperature deactivation processes, a concept of bimetallic Pd–Rh systems with enhanced metal–metal interaction was proposed [34, 40–47]. Both strong metal–support interaction between palladium and donor sites of alumina, and strong metal–metal interaction between palladium and rhodium were shown to have synergetic effect maintaining the catalytic activity on the appropriate level and significantly improving the thermal stability. Ratio of metals within the bimetallic Pd–Rh nanoparticles affects predictably the mechanism of the catalyzed reactions and overall catalytic performance. In general, the main reactions taking place during the overall process include oxidation of CO by oxygen, partial and complete oxidation of hydrocarbons by oxygen and nitrogen oxide, steam reforming of hydrocarbons and water–gas shift reaction [48, 49]. As we have reported recently [50], contribution of the reactions involving NO increases along with an increase in Rh content in the alloy. Therefore, the thermal stability of the bimetallic species and the surface concentration of rhodium are the key factors determining the catalytic performance of the samples.

It is worth noting that in most cases, pure model supports were used to study the effect of metal–support interaction on the catalytic behavior. On the other hand, such materials are of rare application due to their non-satisfactory exploitation properties. For instance, pure γ-$Al_2O_3$ is known to undergo phase transformations within a temperature range of 900–1100 °C, while this range is quite important for usage of TWC, and the support is required to provide appropriate resistance towards aging at such temperatures. From this point of view, thermally stabilized modifications of γ-$Al_2O_3$ are more attractive for manufacturers. Among them, alumina doped with lanthanum oxide is the most usually applied one [51–55]. It should be mentioned that introduction of dopant into alumina lattice also changes the mechanism of metal–support interaction. In particular, rhodium ions still diffuse into the bulk, but the preferable places of their location are quite different [56, 57]. In this case, rhodium is localized at nearest coordination environment of the La cations. Presence of $La^{3+}$ ions within the alumina lattice creates new diffusion pathways for rhodium ions, thus accelerating the rate of their diffusion. Thereby, the high-temperature behavior of the bimetallic Pd–Rh nanoparticles supported on the La-doped alumina is of special interest.

In the present work, the most attention was paid to the investigation of the bimetallic Pd–Rh/(γ$Al_2O_3$ + 4 wt% $La_2O_3$) system in comparison with monometallic Pd-only and Rh-only reference samples, as well as with bimetallic catalyst of the same composition obtained by mechanical mixing of monometallic samples with doubled metal loading (no metal–metal interaction). In order to elucidate the effect of metal–support interactions, the support was calcined at 800 °C prior the deposition of precious metals. Commercial bimetallic TWC containing the same amount of metals was used as a general reference sample. The support and the catalysts were characterized by a number of physicochemical methods.

## 2 Experimental

### 2.1 Synthesis of the Samples

Commercial $La_2O_3$-doped γ-$Al_2O_3$ (TM 100/150 L4, Sasol) containing 4 wt% of lanthanum oxide was taken as a support. The initial support was labeled as L4. Commercial solutions of rhodium and palladium nitrates (JSC «Krastsvetmet», Krasnoyarsk, Russia) were used as salts-precursors.

The samples of alumina-supported bimetallic catalysts with an atomic Pd:Rh ratio of 3:2 were prepared by an incipient wetness impregnation of the L4 support with a joint aqueous solution of rhodium and palladium nitrates. A portion of initially dry powder support was placed into beaker and then preliminary heated solution of the precursor was added dropwise at a constant stirring. The resulting suspension was transferred to a Petri dish and dried in air at room temperature for 12 h. Then, the sample was dried in a furnace at 105 °C for 6 h, heated in air at 550 °C with a temperature ramping rate of 10 °C/min, and maintained at this temperature for 1 h. After cooling, the calcined catalysts were homogenized via grinding in an agate mortar. The total metal loading was 0.35 ± 0.03 wt%. The reference monometallic samples were prepared similarly using single solutions of the corresponding nitrates. The loading of Pd and Rh in the monometallic samples was 0.21 and 0.14 wt%, accordingly. These values correspond to their content in the bimetallic samples. The bimetallic reference sample was obtained by mechanical mixing of specially prepared monometallic samples containing doubled amount of each metal (0.42 and 0.28 wt% of Pd and Rh, respectively). These monometallic samples were taken in equal amounts and mixed in an agate mortar with intensive communication. Additional bimetallic Pd–Rh/L4* sample was prepared by an impregnation of the

L4 support preliminary calcined at 800 °C for 6 h (labeled as L4*) with a joint aqueous solution of rhodium and palladium nitrates followed by all the similar drying and calcination procedures.

Commercial reference sample (CRS) was provided by Ecoalliance LLC (Russia). The powder sample was obtained by stripping the catalytic coating from the honeycomb catalyst and grinding in an agate mortar. Total loading of Pd and Rh in the sample was also 0.35 wt%.

In order to prepare the monolith samples, each powder composition was mixed with water, and subjected to grinding in a beaded mill. The average particle size in the final suspension was about 6–7 microns (D90). The suspension contained 30–35 wt% of solids. Then the suspension was supported on a honeycomb cordierite monolithic substrate RD 4 × 4'' (101.6 mm in diameter and in length, 63 cells/$cm^2$) by an aspiration procedure. The loading of the active composition in the monolith sample was 60 g/$dm^3$. The monolith was dried at 120 °C and calcined at 550 °C for 1 h.

## 2.2 Characterization of the Samples

The textural parameters of the L4 support treated at different conditions (specific surface area, SSA; pore volume, $V_p$; average pore size, $D_{av}$) were determined by a low-temperature nitrogen adsorption/desorption method. Nitrogen adsorption isotherms were obtained at 77 K using an ASAP-2400 automated instrument (Micromeritics, USA). Before the measurements, the samples were kept at the degassing station in a nitrogen flow at 200 °C for 1 h and then cooled down during 0.5 h under the same conditions.

Powder XRD analysis of the L4 support treated at different temperatures was performed at room temperature on a Shimadzu XRD-7000 diffractometer ($CuK_\alpha$ radiation, nickel filter in reflected beam, scintillation detector with amplitude discrimination). Data were collected step-by-step in the range of angles 2θ = 15–70° with a step of 0.1°.

Electron paramagnetic resonance (EPR) spectroscopy was performed using an ERS-221 EPR spectrometer operating in the X-band (ν = 9.3 GHz). EPR spectra were acquired at 20 dB attenuation with typical microwave power 3 mW. Radical anions of aromatic nitro compounds arising from their adsorption on the surface of oxide catalysts were used as spin probes for the study of surface electron-donor sites as described elsewhere [34, 35, 44]. A catalyst sample (~20 mg) was loaded in a quartz ampoule, heated at 170 °C for 12 h, and then cooled down to room temperature. $2 \times 10^{-2}$ M 1,3,5-trinitrobenzene (TNB) solution in toluene was added to launch the formation of the anion radicals. The temperature was then maintained at 80 °C for 12 h for further acceleration of the radical anion formation to their maximum, which corresponds to the concentration of the surface electron-donor sites. The EPR spectra of generated radical anions were recorded at room temperature. The concentrations of the paramagnetic species were determined by a numerical double integration with baseline compensation.

Transmission electron microscopy (TEM) studies were performed using a JEOL JEM-2010 electron microscope (lattice plane resolution 0.14 nm at accelerating voltage of 200 kV). The samples for the TEM study were prepared on perforated carbon film mounted on a copper grid.

Ethane hydrogenolysis reaction was used as a testing reaction to characterize the surface concentration of supported precious metals in reduced state. As it was reported earlier [35, 38], the rate of this reaction linearly depends on the specific surface area of the supported metals. Each sample (100 mg, 0.25–0.5 mm fraction) was placed inside the quartz flow-through reactor. At the beginning of the experiment, a $H_2$/He mixture was passed through the reactor for some time until the system reached a steady state. Then, ethane was added to the feed for a short period of time (3 min) and a probe was taken for chromatographic analysis. During next 10 min the sample was purged by the $H_2$/He mixture flow in order to regenerate the initial steady state. This procedure was repeated for 5 times at each temperature within the studied temperature range with a step of 25 °C.

Diffuse reflectance UV–Vis spectra were recorded between 200 and 800 nm using a UV–Vis spectrometer UV–VIS 2501 PC (Shimadzu) with IRS-250A diffusion reflection attachment. The UV–Vis spectra were transformed into the Kubelka–Munk function F(R) calculated as $F(R) = (1 - R)^2/2R$, where R is the experimentally measured reflectivity coefficient of the samples [58].

X-ray photoelectron spectra (XPS) were recorded on a SPECS spectrometer (Germany) using $MgK_\alpha$ radiation ($h\nu = 1253.6$ eV). Initially, survey spectra of the samples were recorded in a range of binding energies (BE) from 0 to 1000 eV. Then, each spectrum was analyzed and the regions corresponding to the elements presented on the surface were chosen for more precise research. The binding energies were determined with respect to the Al2p line in alumina, which has the energy value equal to 74.5 eV in accordance with the literature [59, 60]. Atomic concentrations of elements were defined relatively to the aluminum concentration with regard to atomic sensitivity factors reported elsewhere [60].

## 2.3 Testing the Catalytic Activity and Thermal Stability

The catalytic performance and thermal stability of the powder catalysts were studied using a prompt thermal aging (PTA) procedure as described elsewhere [34, 44, 47, 58, 61]. CO conversion was used as a chemical response to follow the catalytic behavior and state of active components during the procedure. The sample (300 mg) was loaded into quartz flow reactor, and then the reaction mixture contained

0.15 vol% CO, 14.0 vol% $O_2$ and $N_2$ as balance was passed through the reactor. The flow rate was 334 ml/min. A temperature ramping rate was 10 °C/min. The samples underwent two light-off cycles at 50–320 °C, two cycles at 50–600 °C, two cycles at 50–800 °C, and finally one cycle at 50–400 °C. Changes in the CO concentration in the outlet flow were registered by a gas analyzer ULTRAMAT 6 (Siemens). The temperature of 50% CO conversion was used as a criterion to compare the stability of the catalysts.

Light-off performance studies (temperature of 50% CO, $CH_x$, and $NO_x$ conversion) as well as perturbation tests (maximum conversion in a pulse regime at 400 °C) for the monolith samples were carried out using a Horiba CTSJ-2003.12 analytical setup. The following reaction mixture was passed through the monolith catalyst: 1.15 vol% $O_2$; 1.60 vol% CO; 1000 ppm $NO_x$; 250 ppm $C_3H_6$; 250 ppm $C_3H_8$; 0.4 vol% $H_2$; 9.35 vol% $CO_2$; 10 vol% $H_2O$; $N_2$ as a balance. The gas hourly space velocity (GHSV) was 70000 $h^1$. The sample was heated up in a range of 80–400 °C with ramping rate of 20 °C/min, and was then kept at 400 °C for 3 min.

The operation window of the monolith samples was measured using the same gas mixture as in the previous test (with the exception of $O_2$-oscillation) by scanning Lambda (λ) from 0.97 to 1.01 at temperature of 500 °C. The borders of the operation window were limited by 80% conversion of at least one of three types of contaminants (CO, total hydrocarbons, $NO_x$).

## 3 Results and Discussions

Since the thermal stability of the support is very important in general terms of the catalytic performance of the TWC and in particular to study the metal–support interactions, the initial commercial L4 support was thermally treated at different conditions. Calcination procedure was performed in a muffle furnace in an air atmosphere, while for aging procedure the sample was placed into flow-through reactor and heated up to the corresponding temperature in a flow of air containing 10 vol% of water vapors. Finally, the textural characteristics of the treated samples of the support were examined. The obtained values of specific surface area (SSA), pore volume ($V_p$), and average pore diameter ($D_{av}$) are summarized in Table 1. As seen from the table, each thermal procedure affects the parameters decreasing the SSA and $V_p$ values, and increasing $D_{av}$. More noticeable changes are observed after treating at temperature of 1000 °C and above. Duration of the procedure also has an effect. In average, SSA drops down in 1.5 times, and $D_{av}$ increases in 1.4 times.

The next important factor is a phase composition. Initially, the L4 support is represented by the γ-$Al_2O_3$ phase (space group $Fd\bar{3}m$). The corresponding XRD pattern

**Table 1** Textural characteristics of the L4 support treated at different conditions

| Treatment conditions | SSA ($m^2$/g) | $V_p$ ($cm^3$/g) | $D_{av}$ (Å) |
|---|---|---|---|
| Initial | 157 | 0.928 | 175 |
| Calcination, 800 °C, 1 h | 153 | 0.917 | 178 |
| Calcination, 1000 °C, 1 h | 123 | 0.856 | 191 |
| Aging, 1100 °C, 1 h | 103 | 0.825 | 227 |
| Aging, 1100 °C, 4 h | 91 | 0.791 | 254 |

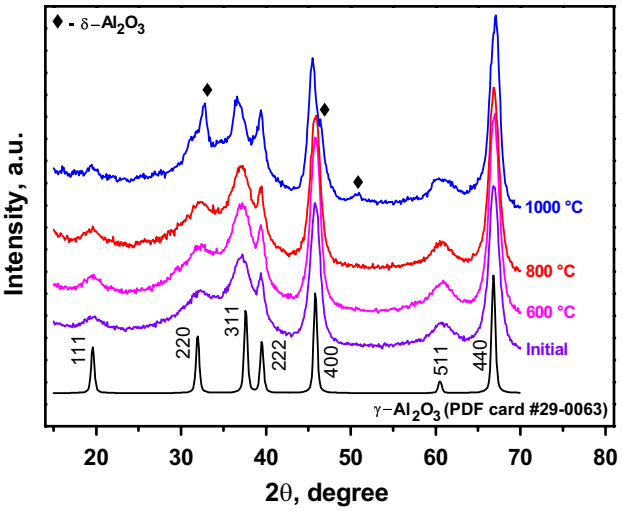


**Fig. 1** XRD patterns of the initial L4 support and after calcination at 600, 800 and 1000 °C for 1 h. Reference pattern for γ-$Al_2O_3$ (JCPDS card No. 29-0063) is presented for comparison

(Fig. 1) demonstrates highly widened diffraction reflexes, and, along with it, the widening of the reflexes assigned to different families of crystalline planes differs strongly. Such behavior is quite typical for pure γ-$Al_2O_3$ support [46]. The XRD patterns for the L4 support calcined at 600 and 800 °C for 1 h are practically coincide with that for the initial sample. The only changes were observed for the sample calcined at 1000 °C. As seen, gamma-phase is particularly transformed into delta-phase (space group $P\bar{4}m2$, PDF card #46-1131) labeled by diamond signs.

The spin probe method based on EPR spectroscopy was recently shown to be informative for characterization of electron-donor sites on the surface of alumina support [35, 46]. Corresponding EPR spectra for the initial and calcined L4 support are presented in Fig. 2. The concentration of radical anions calculated form these spectra are summarized in Table 2. Calcination of the support at 600 °C does not change the situation noticeably. The concentration of donor sites slightly increases, thus indicating the removal of hydroxyl groups initially adsorbed on the surface of the

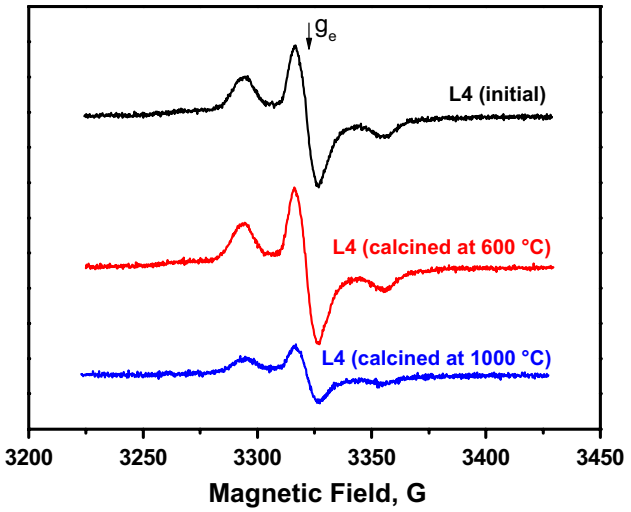


**Fig. 2** EPR spectra for the initial L4 support and after calcination at 600 and 1000 °C for 1 h

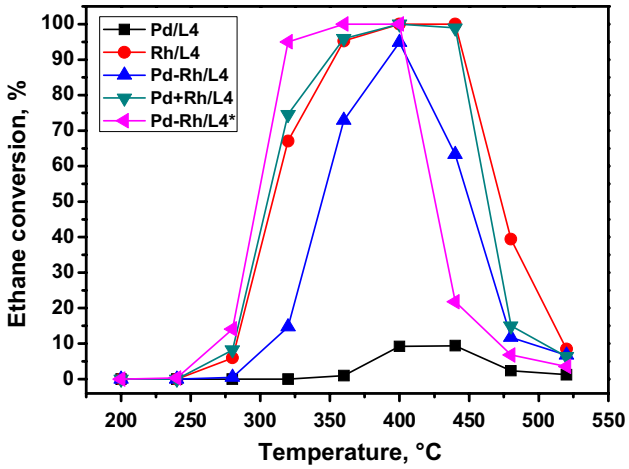


**Fig. 3** Temperature dependences of ethane hydrogenolysis for bimetallic samples Pd–Rh/L4 and Pd–Rh/L4*, and reference samples Pd/L4, Rh/L4 and Pd + Rh/L4. Note that the L4* support was calcined at 800 °C for 6 h on air before impregnation with salts-precursors

**Table 2** Concentration of radical anions for the initial L4 support and after calcination at 600 and 1000 °C for 1 h

| Support | Concentration (spin/g) |
|---|---|
| L4 (initial) | 8.85E17 |
| L4 (calcined at 600 °C) | 9.67822E17 |
| L4 (calcined at 1000 °C) | 3.7037E17 |

support. Calcination at 1000 °C affects the concentration of donor sites more significantly by decreasing this parameter in 2.6 times. Taking into account the correlation reported earlier [35], such decrease in the concentration of donor sites should diminish relatively the amount of palladium species stabilized on the surface.

Samples of the catalysts with deposited precious metals were characterized by a testing reaction of ethane hydrogenolysis. As it was numerously reported by Sinfelt [62–64], kinetics of this reaction strongly depends on the amount of metal atoms in reduced state located on the surface and accessible for the reagents. The characterization technique based on this reaction allows studying the surface of the catalysts with supported metals, measuring of their surface concentration, and estimating the dispersity [35, 36, 38]. Temperature dependences of ethane hydrogenolysis over the studied samples are shown in Fig. 3. Rhodium is much more active in the testing reaction than palladium, and experimental curves corresponding to Rh-containing catalysts lie at significantly lower temperatures if compare with Pd-only sample. Curves for monometallic Rh/L4 and bimetallic Pd + Rh/L4 (obtained by mechanical mixing of separately deposited parts) samples are practically coincide, thus confirming absence of metal–metal interaction in the case of Pd + Rh/L4 sample. Curve for bimetallic Pd–Rh/L4 catalyst (obtained by joint impregnation) is shifted towards higher temperatures due to averaging of the catalytic properties in the bimetallic alloy [44]. Observed descent in conversion values at temperatures above 400 °C is caused by near-surface interactions of metal species with the support, which are reversible. It is important to note that the impregnation of L4* support preliminary calcined at 800 °C with joint solution of palladium and rhodium nitrates does not lead to the formation of Pd–Rh alloy. Catalytic behavior of this sample in the ethane hydrogenolysis reaction evidently illustrates that rhodium is not interacted with palladium. Moreover, the largest amount of metallic Rh on the surface was detected in this case.

Catalytic performance of the studied samples in the target reactions is quite different. The results of PTA tests are presented in Fig. 4 and Table 3. Monometallic Pd/L4 catalyst shows high initial activity (Fig. 4a). After the first catalytic cycle, the $T_{50}$ value increases by 33 °C due to changes of the catalyst's surface state under the reaction conditions, which are mostly caused by dehydroxylation of the surface [37, 65]. Heating of the sample up to 600 °C leads to its deactivation reflected in a further shift of the light-off curves. Then, the sample demonstrates stable behavior, even after aging at 800 °C. Monometallic Rh/L4 sample is less active in comparison with Pd-only sample (Fig. 4b). Difference in the corresponding $T_{50}$ values reaches 150 °C (Table 3). Contrary to Pd-only sample, catalytic activity of Rh/L4 sample in first five cycles is completely reproducible. Aging at 800 °C deactivates the sample, and the $T_{50}$ values are increased by ~ 15 °C. Bimetallic reference sample Pd + Rh/L4 prepared by mechanical mixing exhibits all three deactivation steps (Fig. 4d): low-temperature dehydroxylation, and

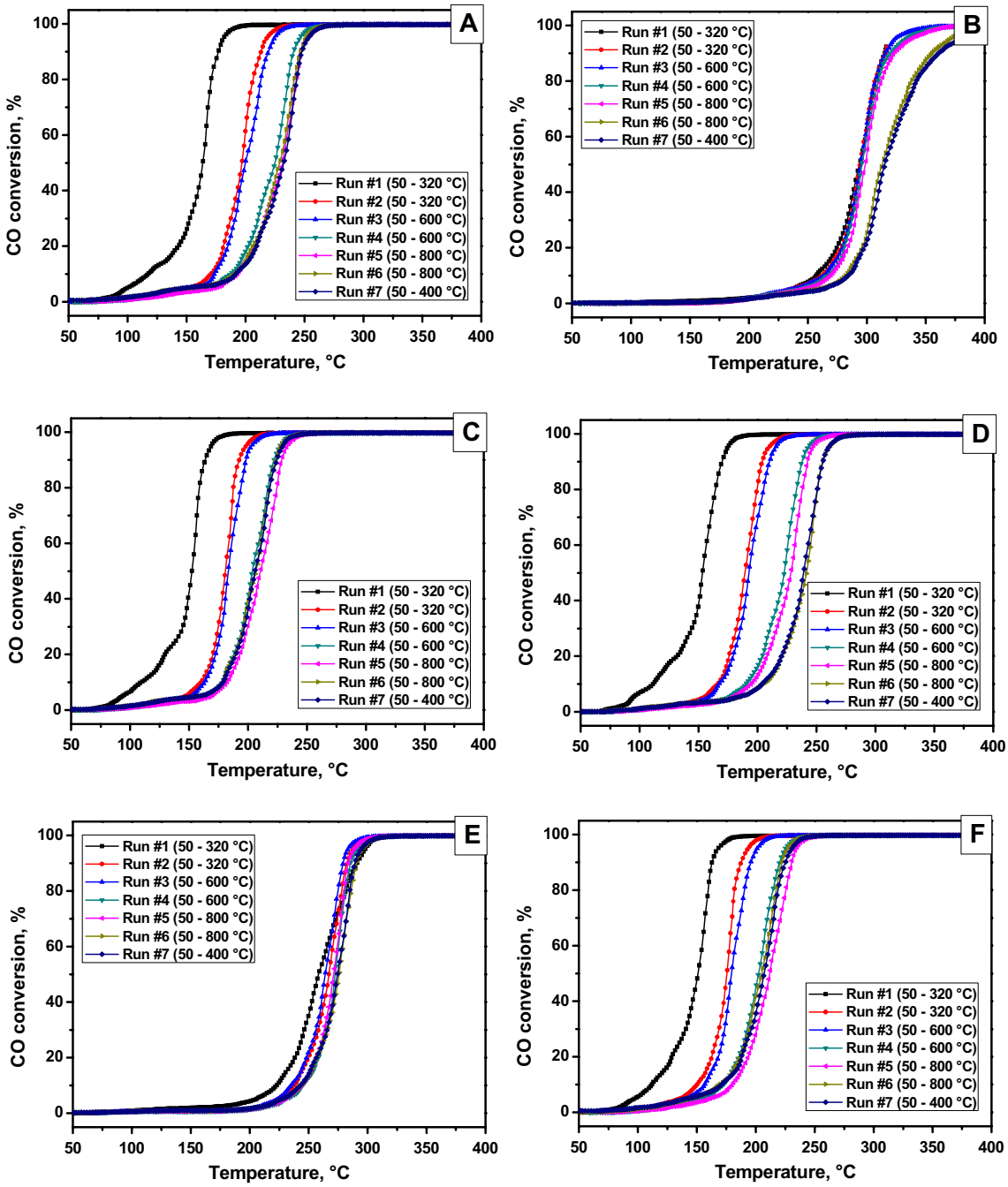


**Fig. 4** Light-off curves of CO conversion at PTA conditions for the studied samples Pd/L4 (**a**), Rh/L4 (**b**), Pd–Rh/L4 (**c**), Pd + Rh/L4 (**d**), Pd–Rh/L4* (**e**), and commercial reference sample CRS (**f**)

high-temperature deactivation after aging at 600 and 800 °C. Thermal stability of bimetallic Pd–Rh/L4 sample is similar to that for Pd-only sample, but catalytic activity is noticeably higher. The $T_{50}$ value in the seventh cycle is 206 °C, which is better than for all other studied catalysts. It should be noted that, in terms of catalytic performance, Pd–Rh/L4 sample is very close to CRS (Table 3). Unusual catalytic behavior was shown by PdRh/L4* sample (Fig. 4e): difference between all catalytic cycles is minimal, but activity (the $T_{50}$ value) is the lowest among all the Pd-containing catalysts. As it follows from results of the ethane hydrogenolysis testing reaction, in this case, no alloy formation has occurred. It was recently reported that both palladium and rhodium prefer the same sites on the surface of the alumina support to interact with [35, 45]. These sites were found to be electron-donor ones. The strength of metal–support interaction and, therefore,

**Table 3** The $T_{50}$ values in seven consecutive cycles at PTA conditions for all the tested samples

| Sample | $T_{50}$ (°C) | | | | | | |
|---|---|---|---|---|---|---|---|
| | 1 | 2 | 3 | 4 | 5 | 6 | 7 |
| CRS | 151 | 176 | 180 | 203 | 212 | 205 | 207 |
| Pd/L4 | 164 | 197 | 200 | 225 | 231 | 229 | 232 |
| Rh/L4 | 294 | 295 | 294 | 296 | 299 | 313 | 315 |
| Pd–Rh/L4 | 152 | 180 | 183 | 204 | 211 | 206 | 206 |
| Pd + Rh/L4 | 154 | 190 | 193 | 223 | 228 | 242 | 240 |
| Pd–Rh/L4* | 259 | 267 | 264 | 273 | 272 | 276 | 275 |

an efficiency of stabilization of metals on the surface are determined by the amount of these sites. Calcination of the L4 support at elevated temperatures even for a short period of time, in its turn, leads to significant decrease in the concentration of donor sites (Table 2). Thereby, the conditions required for proper localization of both metals near the same sites, which is expected to be crucial for alloy formation, are not being realized. Finally, the tendency of appearance of more coarse particles predominantly consisting of single metals is prevailing. These particles are less susceptible to changes during the catalytic cycles, thus providing sustainable catalytic performance. Unfortunately, their activity is discontented.

In order to study the evolution of the palladium species state during the high-temperature treatment, the Pd-containing samples calcined at 600, 800 and 1000 °C were characterized by diffuse reflectance UV–Vis spectroscopy. Calcination of the samples was performed in a muffle furnace for 6 h, which corresponds to more drastic conditions required for realization of such processes as surface migration of palladium and bulk diffusion of rhodium. As it was recently reported [58], the spectra for the $Pd/Al_2O_3$ samples recorded under atmospheric conditions give overestimated values of $E_g$ (band gap) for oxide clusters and small PdO particles, when calculated in accordance with the Tauc approach. To avoid it, the initial state of the catalysts was qualitatively analyzed comparing the shape of the d–d transition bands with normalization Gauss function with a characteristic value of FWHM = 0.71 eV that corresponds to the d–d transition band for isolated $Pd^{2+}$ ions. The spectra shown in Fig. 5a were normalized in amplitude to 1.0 in the area of the d–d transition for $Pd^{2+}$. As seen, a broadening of the d–d transition band in relation to Gauss function is observed for all the examined samples, thus testifying towards formation of small PdO particles. As it was already mentioned, Pd + Rh/L4 catalyst was prepared by mixing of separately synthesized Pd/L4 and Rh/L4 samples with doubled metal loading. In such case, the concentration of supporting metals can exceed the amount of electron-donor sites on the surface of the support. This leads to formation of PdO particles, which is seen in the UV–Vis spectra. No noticeable changes were observed for the samples calcined at 800 °C. After calcination of the samples at 1000 °C (Fig. 5b), the characteristic values of F(R) in the area of the d–d transitions for $Pd^{2+}$ remain the same as for the samples calcined at 600 °C (~ 0.7). At the same time, the long-wavelength edge of the absorption band was restructured, which is typical for PdO particles. In this case, average size of the PdO particles can be characterized by the value of band gap ($E_g$) estimated in accordance with the Tauc approach. Corresponding UV–Vis spectra are presented in Fig. 5c. According to the data obtained, average size of PdO particles has increased in all the cases. However, the smallest value of band gap ($E_g$ = 2.05 eV) was observed for Pd–Rh/L4 sample, while the largest value of 2.13 eV was found for Pd + Rh/L4 sample.

The samples aged at 1000 °C were investigated by TEM method. Figure 6 shows the TEM images obtained. Palladium was found to be distributed within Pd/L4 sample in a wide range of particle sizes: from small clusters of few nm (Fig. 6b) to relatively large agglomerates of tens nm (Fig. 6a). All this correlates well with the data of UV–Vis spectroscopy and results of the PTA tests showing agglomeration of the Pd species during the high-temperature aging. Rhodium in the Rh-only catalyst (Fig. 6c) is represented by particles of 2–3 nm in size, which are strongly interacted with the support. Sample prepared by the impregnation of the support with joint solution of Pd and Rh nitrates (Pd–Rh/L4) contains mostly bimetallic nanoparticles of 10–40 nm in size with Pd:Rh ratio varied from 5:4 to 4:1. An example of such particle consisting of 80% Pd and 20% Rh is shown in Fig. 6d. No large agglomerates as in the case of Pd/L4 sample were found for this catalyst. Thereby, TEM studies confirm a near surface stabilization of rhodium in Rh/L4 sample and a mutual anchoring of Pd and Rh in the bimetallic Pd–Rh/L4 sample.

The effect of the preliminary calcination of the support on the state of supported metals was more precisely studied by means of XPS technique. The XPS spectra recorded in a Pd3d region are shown in Fig. 7a. Despite the small loading of palladium in the samples, the Pd3d band is well resolved. The values of binding energy (BE) for the $Pd3d_{5/2}$ band are 335.8 and 336.0 eV for PdRh/L4 and PdRh/L4* samples, respectively (Table 4). The samples aged at 1000 °C were used for this study. It should be noted that BE for

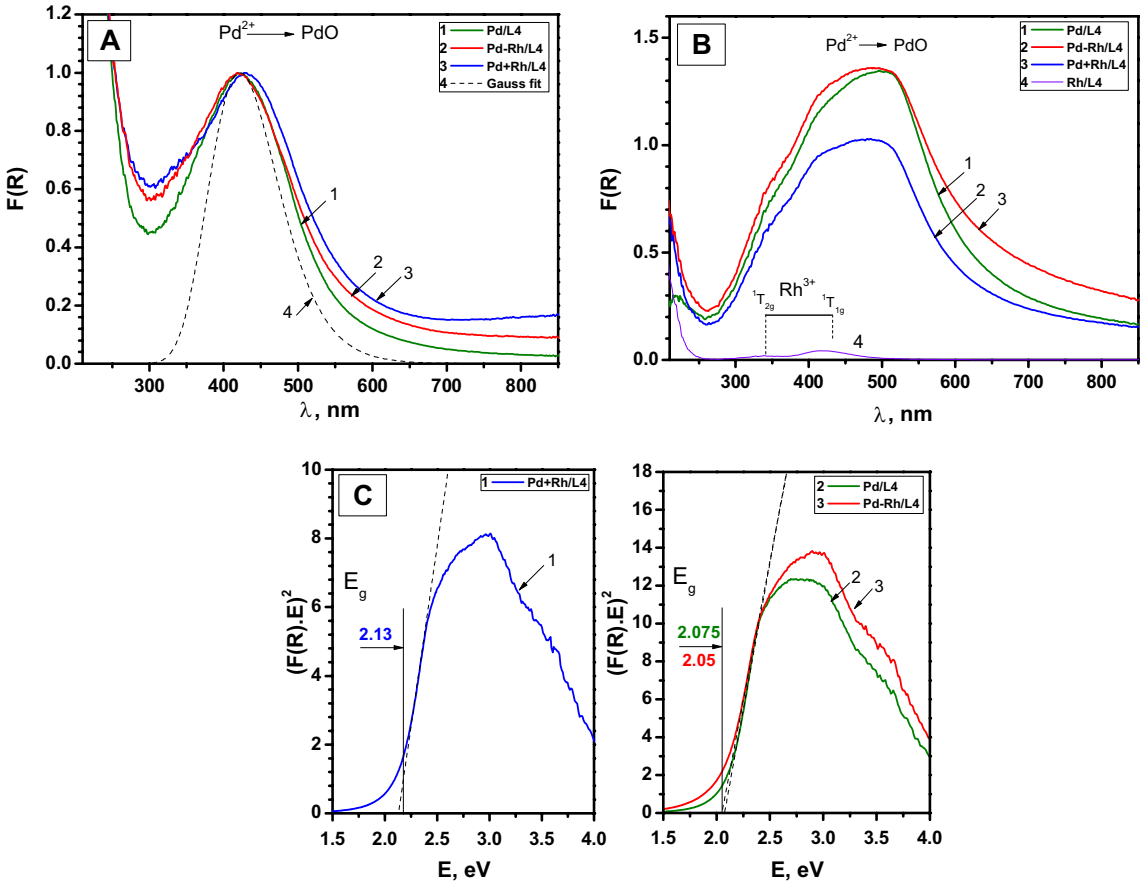


**Fig. 5** Diffuse reflectance UV–Vis spectra for the samples Pd/L4, Pd–Rh/L4, and Pd + Rh/L4 calcined at 600 °C (**a**) and 1000 °C (**b**); diffuse reflectance UV–Vis spectra plotted in the coordinates of $(F(R)\cdot E)^2$ versus E for the same samples calcined at 1000 °C (**c**)

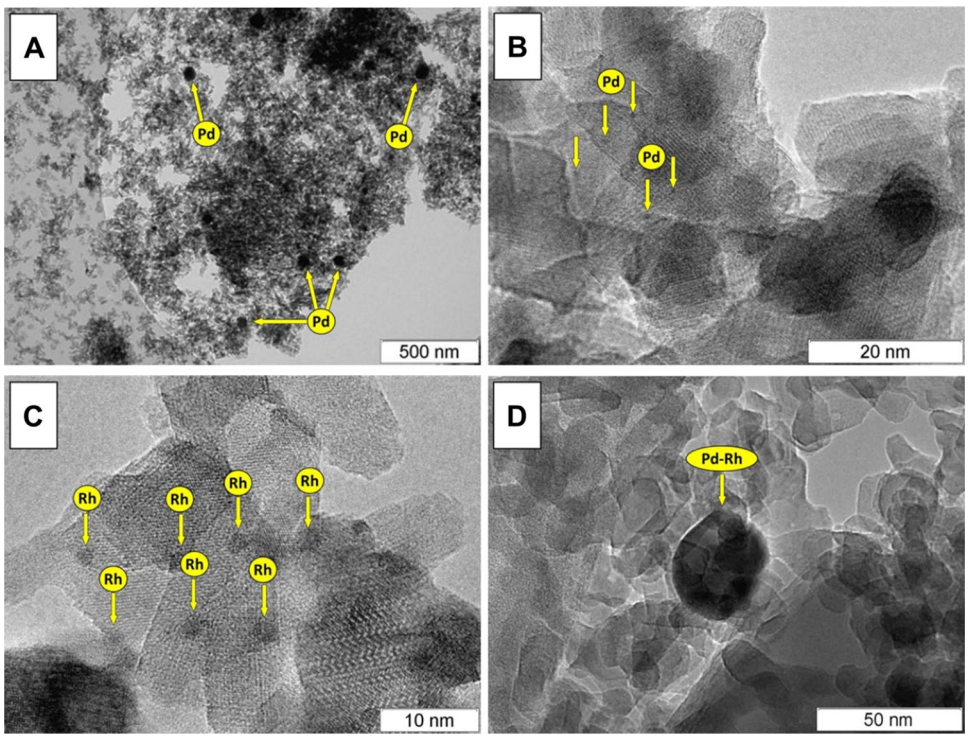


**Fig. 6** TEM images for the samples Pd/L4 (**a**, **b**), Rh/L4 (**c**), and Pd–Rh/L4 (**d**) after aging at 1000 °C

**Table 4** Binding energies of the photoemission bands (eV)

| Sample | $Pd3d_{5/2}$ | $Rh3d_{5/2}$ | $La3d_{5/2}$ | O1s |
|---|---|---|---|---|
| Pd–Rh/L4 | 335.8 | 306.9<br>309.5 | 835.4<br>838.8 | 530.6<br>532.3 |
| Pd–Rh/L4* | 336.0 | 307.8<br>310.0 | 835.6<br>839.0 | 531.8 |

metallic palladium corresponds to 335.1–335.3 eV, while for PdO oxide the values are 336.8–337.0 eV [29, 59, 66–69]. Thereby, the observed values of BE can be assigned to the relatively small particle of metallic palladium [70]. Despite both the samples contain the same amount of palladium, atomic ratios [Pd]/[Al] determined from the XPS spectra are strongly different (Table 5). Preliminary calcination of the support at 800 °C (sample Pd–Rh/L4*) leads to significantly much lower atomic ratio [Pd]/[Al] in the catalyst after aging at 1000 °C. Decrease in intensity of the XPS spectra at constant metal content is known to be typical for the case of the particles enlargement [71, 72]. Thereby, this testifies towards a presence of larger palladium particles, thus confirming less thermal stability of Pd particles on the support's surface and their rapid agglomeration at elevated temperatures observed by previous characterization methods.

**Table 5** Quantitative composition of the surface

| Sample | [Pd]/[Al] | [Rh]/[Al] | $\%RhO_x$ | [La]/[Al] |
|---|---|---|---|---|
| Pd–Rh/L4 | 0.00117 | 0.00185 | 76.9 | 0.0576 |
| Pd–Rh/L4* | 0.00046 | 0.00166 | 80.7 | 0.0660 |

The XPS spectra for Rh3d region are shown in Fig. 7b. These spectra are represented by two duplet bands with BE $Rh3d_{5/2}$ of ~ 307.4 and ~ 309.8 eV (Table 4). The first band can be assigned to nanosized particles of metallic rhodium [59, 60]. BE of the second band belongs to a range of 309.3–310.1 eV, which is typical for $RhO_2$ oxide species [73, 74]. Since BE of $Rh_2O_3$ should correspond to an interval of 307.9–308.6 eV [73–75], absence of such bands allows one to exclude this oxide from the composition of the samples. Atomic ratio [Rh]/[Al] for total rhodium content in the samples and fraction of oxidized Rh species are summarized in Table 5. It is evident that after the high-temperature aging the most part of rhodium exists in the oxide form. Similarly to the case of palladium, atomic ratios [Rh]/[Al] for the samples are different. At the same time, this difference is not so high, and the effect of preliminary calcination of the support on the atomic ratio is insignificant.

Figure 7c demonstrates the XPS spectra for La3d region. The shape of the spectra is represented by two

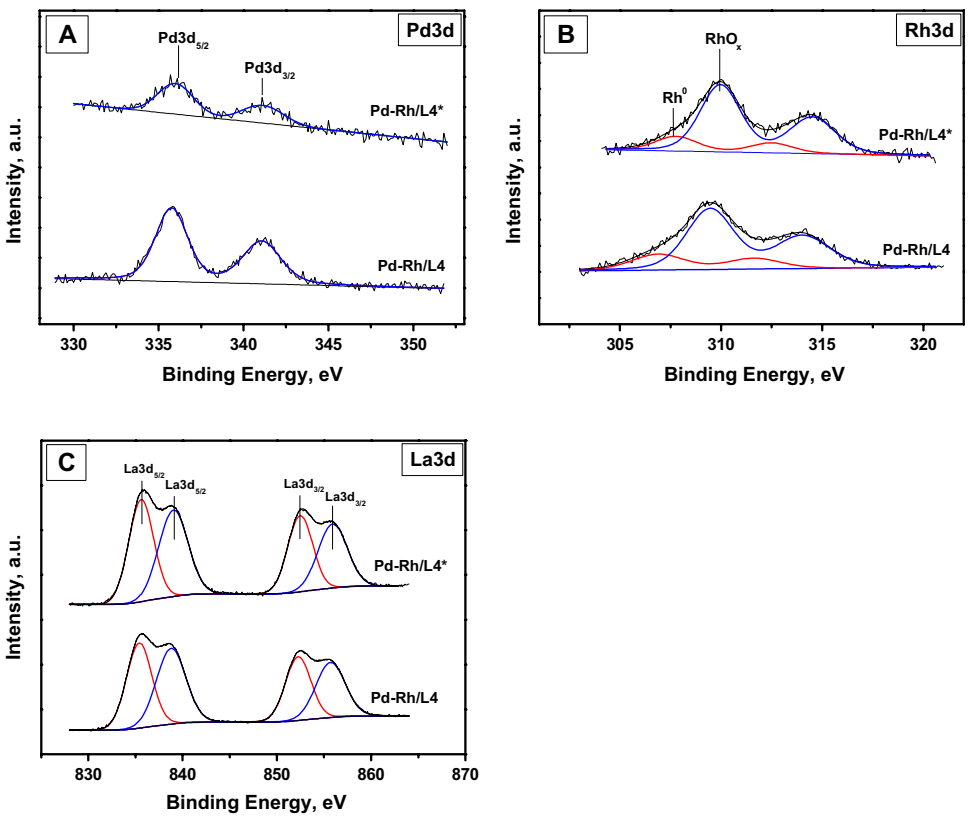


**Fig. 7** XPS spectra for the Pd–Rh/L4 and Pd–Rh/L4* samples aged at 1000 °C: Pd3d region (**a**); Rh3d region (**b**); La3d region (**c**)

doublets with spin–orbit splitting in each of 16.8 eV that is typical for compounds with $La^{3+}$, in particular, $La_2O_3$ [76]. The BE values for $La3d_{5/2}$ bands in each doublet are almost the same (Table 4). Atomic ratios [La]/[Al], which characterize the relative surface concentration of lanthanum, are also similar and correspond to ~ 0.056–0.066 (Table 5). Note that according to the technical data, this ratio should be 0.012. Thereby, an enrichment of the surface with La takes place in both the cases. Since rhodium prefers to be localized near $La^{3+}$ ions [56, 57], such redistribution of La within alumina matrix can be considered as an explanation of the near-surface localization of rhodium and its improved thermal stability.

Bimetallic catalysts Pd–Rh/L4 and Pd + Rh/L4, obtained by joint impregnation and mechanical mixing, correspondingly, were compared with CRS in the monolith tests. Light-off performance of the prepared monolith samples is shown in Fig. 8. As seen from Fig. 8a, both the studied samples surpass CRS in catalytic activity: temperatures of 50% conversion of CO, $NO_x$ and total hydrocarbons (THC) are noticeably lower for these samples. Comparing the samples with each other it can be noticed that mechanical mixture (Pd + Rh/L4 sample) is slightly more active than Pd–Rh/L4 catalyst in oxidation of hydrocarbons. In terms of CO oxidation and $NO_x$ reduction activity, the situation is opposite. The values of THC, CO, and $NO_x$ conversions at 400 °C are compared in Fig. 8b. In relation to this parameter, Pd + Rh/L4 and CRS catalysts coincide in THC and CO conversions, while Pd–Rh/L4 sample demonstrates better performance. In the case of $NO_x$ conversion, both studied samples surpass the reference one.

Another important parameter characterizing the efficiency of TWCs is operation window. As it follows from Fig. 9, the widths of the operation window for the Pd–Rh/L4 and Pd + Rh/L4 samples are comparable. Both presented

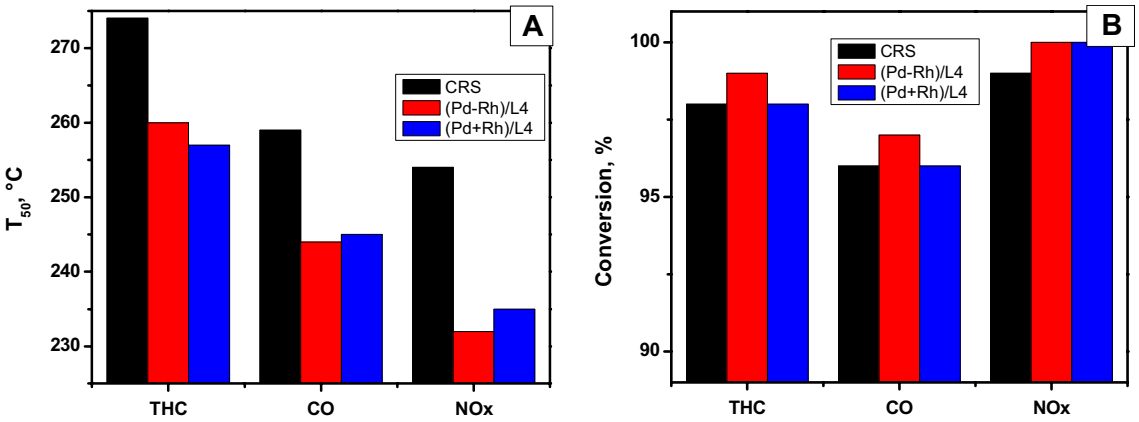


**Fig. 8** Light-off performance of the Pd–Rh/L4, Pd + Rh/L4, and CRS monolith catalysts: $T_{50}$ values of THC, CO, and $NO_x$ conversion (**a**); conversion of THC, CO, and $NO_x$ at 400 °C (**b**)

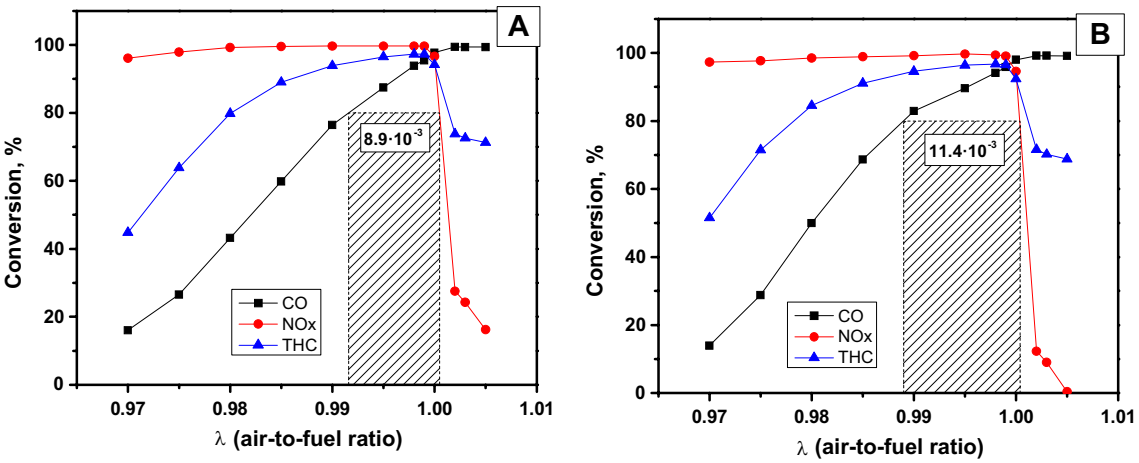


**Fig. 9** Operation window of the monolith catalysts: Pd–Rh/L4 (**a**); Pd + Rh/L4 (**b**)

windows are limited by $NO_x$ and CO conversions. The curve for CO conversion in the case of bimetallic Pd–Rh/L4 sample is mildly sloping, which causes shortening of the window width, thus making this catalyst slightly less effective. On the other hand, the difference is not crucial. For instance, the width of operation window for (0.5 wt%) Rh/CeZrYLa$O_2$ catalyst aged at similar conditions was recently reported to be just 1.3 units [39]. Thus, it can be concluded that the application of bimetallic Pd–Rh/L4 catalysts of alloyed type looks very promising in terms of appropriate catalytic performance and excellent thermal stability.

## 4 Conclusions

Bimetallic Pd–Rh catalysts with strong metal–metal and metal–support interactions attract a growing interest due to enhanced catalytic performance and thermal stability. On the other hand, La-doped $\gamma Al_2O_3$ system used as one of the components of modern three-way catalysts is not precisely studied yet. Thereby, the present work was devoted to detailed study of Pd–Rh/($\gamma Al_2O_3$ + 4 wt% $La_2O_3$) catalyst in comparison with monometallic Pd-only and Rh-only reference samples. In order to investigate the effect of metal–metal interaction, bimetallic sample of the same composition was prepared by mixing separately prepared samples with doubled loading of each metal. The effect of metal–support interaction was studied by comparing the samples with another reference sample synthesized by an impregnation of the preliminary calcined at 800 °C support with a joint solution of rhodium and palladium nitrates. Catalytic performance of the prepared samples was referred to that for the sample of commercial catalyst.

Doping of alumina with lanthanum oxide is known to be efficient for improvement of the thermal stability of the support. At the same time, properties of thermally stabilized alumina are being changed after calcination or aging at temperatures of 1000 °C and above. In particular, the value of specific surface area is dropped down significantly, reflexes of the δ-phase are appeared in the XRD patterns, and the concentration of the surface electron-donor sites is decreased. Changes in the support's surface properties during the thermal treatment affect the localization of metals on the impregnation stage and the catalytic properties of the final catalysts. Thus, in the case of initial support, its impregnation with joint solution of Pd and Rh nitrates results in formation of the Pd–Rh alloyed nanoparticles strongly interacted with the support. Preliminary calcination of the support at already 800 °C changes the preferable localization of metals during the same procedure, and the alloy is not being formed, since metals do not interact with each other. Moreover, interaction of metals with the support became significantly weaker. Such catalyst exhibits the worse catalytic activity and thermal stability. Another bimetallic Pd + Rh/L4 sample (mechanical mixture) with no metal–metal interaction was found to be characterized by good enough initial activity, but quite poor thermal stability. Contrary, bimetallic Pd–Rh/L4 catalyst of alloyed type has shown excellent stability and catalytic activity comparable with the commercial reference sample. Thereby, it can be concluded that the concept of bimetallic Pd–Rh nanoalloys can be efficiently applied in the case of La-doped alumina used in the real three-way catalysts.

**Acknowledgements** The study was financially supported by the Ministry of Education and Science of the Russian Federation within the framework of subsidizing agreement of October 23, 2017 (No. 14.581.21.0028, unique agreement identifier RFMEFI58117×0028) of the Federal Target Program "Research and development in priority directions of the progress of the scientific and technological complex of Russia for the years 2014–2020. Characterization of the samples was performed using the equipment of the Center of Collective Use "National Center of Catalysts Research".

### Compliance with Ethical Standards

**Conflict of Interest** The authors declare that they have no conflict of interest.

## References

1. Matsumoto S (1997) Recent advances in automobile exhaust catalyst. Catal Survey Japan 1:111–117. https://doi.org/10.1023/a:1019044022843
2. Gandhi HS, Graham GW, McCabe RW (2003) Automotive exhaust catalysis. J Catal 216:433–442. https://doi.org/10.1016/s0021-9517(02)00067-2
3. Twigg MV (2005) Controlling automotive exhaust emissions: successes and underlying science. Philos T R Soc A 363:1013–1033. https://doi.org/10.1098/rsta.2005.1547
4. Matsumoto S (2007) Advances in automobile exhaust catalyst. Stud Surf Sci Catal 172:27–34
5. Bera P, Hegde MS (2010) Recent advances in auto exhaust catalysis. J Indian Inst Sci 90:299–325
6. Heck RM, Farrauto RJ, Gulati ST (2009) Catalytic air pollution control. Wiley, New York. https://doi.org/10.1002/9781118397749
7. Taylor KC (1984) Automobile catalytic converters. Advances in comparative and environmental physiology. Advances in comparative and environmental physiology. Springer, Berlin, pp 119–170. https://doi.org/10.1007/978-3-642-93247-2_2
8. Fornasiero P, Dimonte R, Rao GR, Kaspar J, Meriani S, Trovarelli A, Graziani M (1995) Rh-loaded CeO2-ZrO2 solid-solutions as highly efficient oxygen exchangers: dependence of the reduction behavior and the oxygen storage capacity on the structural-properties. J Catal 151:168–177. https://doi.org/10.1006/jcat.1995.1019
9. Vidmar P, Fornasiero P, Kašpar J, Gubitosa G, Graziani M (1997) Effects of trivalent dopants on the redox properties of Ce0.6Zr0.4O2 mixed oxide. J Catal 171:160–168. https://doi.org/10.1006/jcat.1997.1784

10. Vlaic G, Fornasiero P, Geremia S, Kašpar J, Graziani M (1997) Relationship between the zirconia-promoted reduction in the Rh-loaded Ce0.5Zr0.5O2 mixed oxide and the Zr–O local structure. J Catal 168:386–392. https://doi.org/10.1006/jcat.1997.1644
11. Fornasiero P, Kašpar J, Graziani M (1999) On the rate determining step in the reduction of CeO2–ZrO2 mixed oxides. Appl Catal B 22:L11–L14. https://doi.org/10.1016/s0926-3373(99)00038-7
12. Graham GW, Jen HW, Chun W, McCabe RW (1999) High-temperature-aging-induced encapsulation of metal particles by support materials: comparative results for Pt, Pd, and Rh on cerium–zirconium mixed oxides. J Catal 182:228–233. https://doi.org/10.1006/jcat.1998.2328
13. Kašpar J, Fornasiero P, Graziani M (1999) Use of $CeO_2$-based oxides in the three-way catalysis. Catal Today 50:285–298. https://doi.org/10.1016/s0920-5861(98)00510-0
14. Shelef M, McCabe RW (2000) Twenty-five years after introduction of automotive catalysts: what next? Catal Today 62:35–50. https://doi.org/10.1016/s0920-5861(00)00407-7
15. Di Monte R, Fornasiero P, Kašpar J, Graziani M, Gatica JM, Bernal S, Gómez-Herrero A (2000) Stabilisation of nanostructured $Ce_{0.2}Zr_{0.8}O_2$ solid solution by impregnation on $Al_2O_3$: a suitable method for the production of thermally stable oxygen storage/release promoters for three-way catalysts. Chem Commun 21:2167–2168. https://doi.org/10.1039/b006674p
16. Kašpar J, Fornasiero P, Hickey N (2003) Automotive catalytic converters: current status and some perspectives. Catal Today 77:419–449. https://doi.org/10.1016/s0920-5861(02)00384-x
17. Maillet T, Solleau C, Barbier J, Duprez D (1997) Oxidation of carbon monoxide, propene, propane and methane over a Pd/Al2O3 catalyst. Effect of the chemical state of Pd. Appl Catal B 14:85–95. https://doi.org/10.1016/s0926-3373(97)00014-3
18. Datye AK, Bravo J, Nelson TR, Atanasova P, Lyubovsky M, Pfefferle L (2000) Catalyst microstructure and methane oxidation reactivity during the Pd ↔ PdO transformation on alumina supports. Appl Catal A 198:179–196. https://doi.org/10.1016/s0926-860x(99)00512-8
19. Monteiro RS, Dieguez LC, Schmal M (2001) The role of Pd precursors in the oxidation of carbon monoxide over $Pd/Al_2O_3$ and $Pd/CeO_2/Al_2O_3$ catalysts. Catal Today 65:77–89. https://doi.org/10.1016/S0920-5861(00)00547-2
20. Matsouka V, Konsolakis M, Yentekakis IV, Papavasiliou A, Tsetsekou A, Boukos N (2011) Thermal aging behavior of Pt-only TWC converters under simulated exhaust conditions: effect of rare earths (CeO2, La2O3) and alkali (Na) modifiers. Top Catal 54:1124–1134. https://doi.org/10.1007/s11244-011-9734-6
21. Busca G, Finocchio E, Escribano VS (2012) Infrared studies of CO oxidation by oxygen and by water over Pt/Al2O3 and Pd/Al2O3 catalysts. Appl Catal B 113–114:172–179. https://doi.org/10.1016/j.apcatb.2011.11.035
22. Fan J, Wu X, Yang L, Weng D (2007) The SMSI between supported platinum and $CeO_2$–$ZrO_2$–$La_2O_3$ mixed oxides in oxidative atmosphere. Catal Today 126:303–312. https://doi.org/10.1016/j.cattod.2007.06.005
23. Beck IE, Bukhtiyarov VI, Pakharukov IY, Zaikovsky VI, Kriventsov VV, Parmon VN (2009) Platinum nanoparticles on Al2O3: correlation between the particle size and activity in total methane oxidation. J Catal 268:60–67. https://doi.org/10.1016/j.jcat.2009.09.001
24. Kwak JH, Hu J, Mei D, Yi CW, Kim DH, Peden CHF, Allard LF, Szanyi J (2009) Coordinatively unsaturated Al3+ centers as binding sites for active catalyst phases of platinum on γ-Al2O3. Science 325:1670–1673. https://doi.org/10.1126/science.1176745
25. Shelef M, Graham GW (2006) Why rhodium in automotive three-way catalysts? Catal Rev 36:433–457. https://doi.org/10.1080/01614949408009468
26. Van CZ, Dettling JC (1987) Rhodium–support interactions in automotive exhaust catalysts. In: Catalysis and automotive pollution control, proceedings of the first international symposium (CAPOC I). Stud Surf Sci Catal, pp 369–386. https://doi.org/10.1016/s0167-2991(09)60436-5
27. Ciuparu D (2000) Pd–Ce interactions and adsorption properties of palladium: CO and NO TPD studies over Pd–Ce/Al2O3 catalysts. Appl Catal B 26:241–255. https://doi.org/10.1016/s0926-3373(00)00130-2
28. Boronin AI, Slavinskaya EM, Danilova IG, Gulyaev RV, Amosov YI, Kuznetsov PA, Polukhina IA, Koscheev SV, Zaikovskii VI, Noskov AS (2009) Investigation of palladium interaction with cerium oxide and its state in catalysts for low-temperature CO oxidation. Catal Today 144:201–211. https://doi.org/10.1016/j.cattod.2009.01.035
29. Luo J-Y, Meng M, Xian H, Tu Y-B, Li X-G, Ding T (2009) The nanomorphology-controlled palladium–support interaction and the catalytic performance of Pd/CeO2 catalysts. Catal Lett 133:328–333. https://doi.org/10.1007/s10562-009-0194-6
30. Hinokuma S, Fujii H, Okamoto M, Ikeue K, Machida M (2010) Metallic Pd nanoparticles formed by Pd–O–Ce interaction: a reason for sintering-induced activation for CO oxidation. Chem Mater 22:6183–6190. https://doi.org/10.1021/cm102355x
31. Zheng T, He J, Zhao Y, Xia W, He J (2014) Precious metal–support interaction in automotive exhaust catalysts. J Rare Earths 32:97–107. https://doi.org/10.1016/s1002-0721(14)60038-7
32. Hegde MS, Bera P (2015) Noble metal ion substituted CeO2 catalysts: electronic interaction between noble metal ions and CeO2 lattice. Catal Today 253:40–50. https://doi.org/10.1016/j.cattod.2015.03.035
33. Alikin EA, Vedyagin AA (2016) High Temperature interaction of rhodium with oxygen storage component in three-way catalysts. Top Catal 59:1033–1038. https://doi.org/10.1007/s11244-016-0585-z
34. Vedyagin AA, Volodin AM, Kenzhin RM, Stoyanovskii VO, Shubin YV, Plyusnin PE, Mishakov IV (2017) Effect of metal–metal and metal–support interaction on activity and stability of Pd–Rh/alumina in CO oxidation. Catal Today 293–294:73–81. https://doi.org/10.1016/j.cattod.2016.10.010
35. Vedyagin AA, Volodin AM, Stoyanovskii VO, Mishakov IV, Medvedev DA, Noskov AS (2011) Characterization of active sites of Pd/Al2O3 model catalysts with low Pd content by luminescence, EPR and ethane hydrogenolysis. Appl Catal B 103:397–403. https://doi.org/10.1016/j.apcatb.2011.02.002
36. Vedyagin A, Volodin A, Kenzhin R, Chesnokov V, Mishakov I (2016) CO oxidation over Pd/ZrO2 catalysts: role of support′s donor sites. Molecules 21:1289. https://doi.org/10.3390/molecules21101289
37. Vedyagin AA, Volodin AM, Kenzhin RM, Stoyanovskii VO, Rogov VA, Kriventsov VV, Mishakov IV (2018) The role of chemisorbed water in formation and stabilization of active sites on Pd/alumina oxidation catalysts. Catal Today 307:102–110. https://doi.org/10.1016/j.cattod.2017.01.033
38. Stoyanovskii VO, Vedyagin AA, Aleshina GI, Volodin AM, Noskov AS (2009) Characterization of Rh/Al2O3 catalysts after calcination at high temperatures under oxidizing conditions by luminescence spectroscopy and catalytic hydrogenolysis. Appl Catal B 90:141–146. https://doi.org/10.1016/j.apcatb.2009.03.003

39. Alikin EA, Denisov SP, Vedyagin AA (2018) Partial regeneration of model TWC after high-temperature aging on engine bench. Top Catal 62:324–330. https://doi.org/10.1007/s11244-018-1114-z
40. Nunan JG, Williamson WB, Robota HJ, Henk MG (1995) Impact of Pt–Rh and Pd–Rh interactions on performance of bimetal catalysts. SAE Tech Paper 950258. https://doi.org/10.4271/950258
41. Araya P, Díaz V (1997) Synergism in the reaction of CO with O2 on bimetallic Rh–Pd catalysts supported on silica. J Chem Soc Faraday Trans 93:3887–3891. https://doi.org/10.1039/a703704j
42. Renzas JR, Huang W, Zhang Y, Grass ME, Hoang DT, Alayoglu S, Butcher DR, Tao F, Liu Z, Somorjai GA (2011) $Rh_{1-x}Pd_x$ nanoparticle composition dependence in CO oxidation by oxygen: catalytic activity enhancement in bimetallic systems. Phys Chem Chem Phys 13:2556–2562. https://doi.org/10.1039/c0cp01858a
43. Renzas JR, Huang W, Zhang Y, Grass ME, Somorjai GA (2010) Rh1–xPdx nanoparticle composition dependence in CO oxidation by NO. Catal Lett 141:235–241. https://doi.org/10.1007/s10562-010-0462-5
44. Vedyagin AA, Gavrilov MS, Volodin AM, Stoyanovskii VO, Slavinskaya EM, Mishakov IV, Shubin YV (2013) Catalytic purification of exhaust gases over Pd–Rh alloy catalysts. Top Catal 56:1008–1014. https://doi.org/10.1007/s11244-013-0064-8
45. Vedyagin AA, Volodin AM, Stoyanovskii VO, Kenzhin RM, Slavinskaya EM, Mishakov IV, Plyusnin PE, Shubin YV (2014) Stabilization of active sites in alloyed Pd–Rh catalysts on $\gamma Al_2O_3$ support. Catal Today 238:80–86. https://doi.org/10.1016/j.cattod.2014.02.056
46. Vedyagin AA, Volodin AM, Stoyanovskii VO, Kenzhin RM, Plyusnin PE, Shubin YV, Mishakov IV (2017) Effect of alumina phase transformation on stability of low-loaded Pd–Rh catalysts for CO oxidation. Top Catal 60:152–161. https://doi.org/10.1007/s11244-016-0726-4
47. Vedyagin AA, Shubin YV, Kenzhin RM, Plyusnin PE, Stoyanovskii VO, Volodin AM (2018) Prospect of using nanoalloys of partly miscible rhodium and palladium in three-way catalysis. Top Catal 62:305–314. https://doi.org/10.1007/s11244-018-1093-0
48. Ma L-P, Bart H-J, Ning P, Zhang A, Wu G, Zengzang Z (2009) Kinetic study of three-way catalyst of automotive exhaust gas: modeling and application. Chem Eng J 155:241–247. https://doi.org/10.1016/j.cej.2009.07.045
49. Kang SB, Han SJ, Nam I-S, Cho BK, Kim CH, Oh SH (2014) Detailed reaction kinetics for double-layered Pd/Rh bimetallic TWC monolith catalyst. Chem Eng J 241:273–287. https://doi.org/10.1016/j.cej.2013.12.039
50. Vedyagin AA, Stoyanovskii VO, Plyusnin PE, Shubin YV, Slavinskaya EM, Mishakov IV (2018) Effect of metal ratio in alumina-supported Pd–Rh nanoalloys on its performance in three way catalysis. J Alloys Compd 749:155–162. https://doi.org/10.1016/j.jallcom.2018.03.250
51. Yang J, Wang Q, Wang T, Liang Y (2016) Rapid preparation process, structure and thermal stability of lanthanum doped alumina aerogels with a high specific surface area. RSC Adv 6:26271–26279. https://doi.org/10.1039/c5ra28053b
52. Barrera A, Fuentes S, Díaz G, Gómez-Cortés A, Tzompantzi F, Molina JC (2012) Methane oxidation over Pd catalysts supported on binary $Al_2O_3$–$La_2O_3$ oxides prepared by the sol–gel method. Fuel 93:136–141. https://doi.org/10.1016/j.fuel.2011.11.049
53. Li M, Weng D, Wu X, Wan J, Wang B (2013) Importance of re-oxidation of palladium by interaction with lanthana for propane combustion over $Pd/Al_2O_3$ catalyst. Catal Today 201:19–24. https://doi.org/10.1016/j.cattod.2012.03.047
54. Zhou Y, Wang Z, Liu C (2015) Perspective on CO oxidation over Pd-based catalysts. Catal Sci Technol 5:69–81. https://doi.org/10.1039/c4cy00983e
55. Lupescu JA, Schwank JW, Dahlberg KA, Seo CY, Fisher GB, Peczonczyk SL, Rhodes K, Jagner MJ, Haack LP (2016) Pd model catalysts: effect of aging environment and lean redispersion. Appl Catal B 183:343–360. https://doi.org/10.1016/j.apcatb.2015.10.018
56. Stoyanovskii VO, Vedyagin AA, Volodin AM, Kenzhin RM, Shubin YV, Plyusnin PE, Mishakov IV (2017) Peculiarity of Rh bulk diffusion in La-doped alumina and its impact on CO oxidation over Rh/Al2O3. Catal Commun 97:18–22. https://doi.org/10.1016/j.catcom.2017.04.013
57. Stoyanovskii VO, Vedyagin AA, Volodin AM, Kenzhin RM, Bespalko YN, Plyusnin PE, Shubin YV (2018) Optical spectroscopy of Rh3+ ions in the lanthanum–aluminum oxide systems. J Lumin 204:609–617. https://doi.org/10.1016/j.jlumin.2018.08.070
58. Stoyanovskii VO, Vedyagin AA, Volodin AM, Kenzhin RM, Slavinskaya EM, Plyusnin PE, Shubin YV (2018) Optical spectroscopy methods in the estimation of the thermal stability of bimetallic Pd–Rh/Al2O3 three-way catalysts. Top Catal 62:296–304. https://doi.org/10.1007/s11244-018-1112-1
59. Nefedov VI (1984) X-ray photoelectron spectroscopy of chemical compounds: handbook. Khimiya, Moscow
60. Moulder JF, Stickle WF, Sobol PE, Bomben KD (1992) Handbook of X-ray photoelectron spectroscopy. Perkin-Elmer Corporation, Eden Prairie
61. Vedyagin AA, Stoyanovskii VO, Kenzhin RM, Slavinskaya EM, Plyusnin PE, Shubin YV (2019) Purification of gasoline exhaust gases using bimetallic Pd–Rh/δ-$Al_2O_3$ catalysts. Reac Kinet Mech Catal 127:137–148. https://doi.org/10.1007/s11144-019-01573-1
62. Sinfelt J, Yates DJC (1967) Catalytic hydrogenolysis of ethane over the noble metals of Group VIII. J Catal 8:82–90. https://doi.org/10.1016/0021-9517(67)90284-9
63. Yates D, Sinfelt JH (1967) The catalytic activity of rhodium in relation to its state of dispersion. J Catal 8:348–358. https://doi.org/10.1016/0021-9517(67)90331-4
64. Sinfelt J (1972) Kinetics of ethane hydrogenolysis. J Catal 27:468–471. https://doi.org/10.1016/0021-9517(72)90188-1
65. Vedyagin AA, Volodin AM, Kenzhin RM, Stoyanovskii VO, Rogov VA, Medvedev DA, Mishakov IV (2017) Characterization and study on the thermal aging behavior of palladium–alumina catalysts. J Therm Anal Calorim 130:1865–1874. https://doi.org/10.1007/s10973-017-6530-y
66. Peuckert M (1985) XPS study on surface and bulk palladium oxide, its thermal stability, and a comparison with other noble metal oxides. J Phys Chem 89:2481–2486. https://doi.org/10.1021/j100258a012
67. Fleisch TH, Zajac GW, Schreiner JO, Mains GJ (1986) An XPS study of the UV photoreduction of transition and noble metal oxides. Appl Surf Sci 26:488–497. https://doi.org/10.1016/0169-4332(86)90120-0
68. Fox EB, Lee AF, Wilson K, Song C (2008) In-situ XPS study on the reducibility of Pd-promoted Cu/CeO2 catalysts for the oxygen-assisted water–gas-shift reaction. Top Catal 49:89–96. https://doi.org/10.1007/s11244-008-9063-6
69. Devener BV, Anderson SL, Shimizu T, Wang H, Nabity J, Engel J, Yu J, Wickham D, Williams S (2009) In situ generation of Pd/PdO nanoparticle methane combustion catalyst: correlation of particle surface chemistry with ignition. J Phys Chem C 113:20632–20639. https://doi.org/10.1021/jp904317y

70. Mason MG (1983) Electronic structure of supported small metal clusters. Phys Rev B 27:748–762. https://doi.org/10.1103/PhysRevB.27.748
71. Beketov G, Heinrichs B, Pirard JP, Chenakin S, Kruse N (2013) XPS structural characterization of Pd/SiO2 catalysts prepared by cogelation. Appl Surf Sci 287:293–298. https://doi.org/10.1016/j.apsusc.2013.09.145
72. Weng X, Shi B, Liu A, Sun J, Xiong Y, Wan H, Zheng S, Dong L, Chen Y-w (2019) Highly dispersed Pd/modified-Al2O3 catalyst on complete oxidation of toluene: role of basic sites and mechanism insight. Appl Surf Sci 497:143747. https://doi.org/10.1016/j.apsusc.2019.143747
73. Weng-Sieh Z, Gronsky R, Bell AT (1997) Microstructural evolution of γ-alumina-supported Rh upon aging in air. J Catal 170:62–74. https://doi.org/10.1006/jcat.1997.1738
74. Suhonen S, Valden M, Hietikko M, Laitinen R, Savimäki A, Härkönen M (2001) Effect of Ce–Zr mixed oxides on the chemical state of Rh in alumina supported automotive exhaust catalysts studied by XPS and XRD. Appl Catal A 218:151–160. https://doi.org/10.1016/s0926-860x(01)00636-6
75. Tolia AA, Smiley RJ, Delgass WN, Takoudis CG, Weaver MJ (1994) Surface oxidation of rhodium at ambient pressures as probed by surface-enhanced Raman and X-ray photoelectron spectroscopies. J Catal 150:56–70. https://doi.org/10.1006/jcat.1994.1322
76. Wanger CD, Riggs WM, Davis LE, Moulder JF, Muilenberg GE (1979) Handbook of X-ray photoelectron spectroscopy. Perkin-Elmer Corp., Eden Prairie